Nanostructured Mg for hydrogen production by hydrolysis obtained by MgH2 milling and dehydriding

Santiago A. Pighin, Guillermina Urretavizcaya, Jean-Louis Bobet, Facundo J. Castro

Nanostructured Mg for hydrogen production by hydrolysis obtained by MgH_2 milling and dehydriding

S.A. Pighin[a,b,*], G.Urretavizcaya[a,c], J.-L. Bobet[d], F.J. Castro[a,c]

[a] CNEA, CONICET, Centro Atómico Bariloche, S.C. de Bariloche, Río Negro, Argentina.
[b] Universidad Nacional del Comahue, Centro Regional Universitario Bariloche, S.C. de Bariloche, Río Negro, Argentina.
[c] Universidad Nacional de Cuyo, Instituto Balseiro, S.C. Bariloche, Río Negro, Argentina.
[d] University of Bordeaux, CNRS, Bordeaux INP, ICMCB, UMR 5026, F-33600 Pessac, France.

* Corresponding author. CNEA, CONICET, Centro Atómico Bariloche, S.C. de Bariloche, Río Negro, Argentina. E-mail address: spighin@cab.cnea.gov.ar (S.A. Pighin).

Abstract

The synthesis, characterization and hydrolysis properties of nanostructured MgH_2 and Mg in a 0.6 M $MgCl_2$ aqueous solution are reported. The microstructural properties of commercial MgH_2 are modified by mechanical milling without additives under H_2 atmosphere for 5 h. The nanostructured Mg is obtained by dehydriding the as-milled MgH_2 under vacuum at 355 °C for 2.5 h. The as-milled MgH_2 shows average hydrolysis properties with good hydrogen production capacity (1390 mL/g H_2) and kinetics (50% of the total yield in 2.3 min). The nanostructured Mg exhibits excellent hydrolysis properties with a high yield (910 mL/g H_2), fast kinetics (90% of the total yield in 2.6 min) and practically no effect of a $MgO/Mg(OH)_2$ passivating layer. The hydrolysis properties of both materials are attributed to their morphology and microstructure. The activation energies of the reaction are estimated and the mechanisms are discussed.

Keywords

Hydrogen generation
Hydrolysis
Mg-based materials
Reaction kinetics
Ball milling

1 Introduction

In a context of environmental and energy issues, mobiles and small portable applications would be greatly enhanced if they could be powered by a hydrogen fuel cell coupled to a hydrogen source that provides the fuel on demand. To this end, the hydrogen supply has to fulfill several conditions, such as to operate under mild conditions, be safe, environmentally friendly, light, compact, and affordable. An attractive way to accomplish these requirements is to take advantage of the hydrolysis of a Mg-based material. This can be achieved by the hydrolysis reaction in presence of the metal:

$$Mg + 2H_2O \rightarrow Mg(OH)_2 + H_2 \quad (1)$$

or its hydride:

$$MgH_2 + 2H_2O \rightarrow Mg(OH)_2 + 2H_2 \quad (2)$$

These options exhibit low security concerns, as hydrogen is not stored as a gas but produced on demand by putting into contact the material with water, and is non-contaminant because reactants and products are innocuous. Additionally, 1020 and 1880 mL/g of hydrogen can be produced from reactions (1) and (2) at 1 bar and 25 °C, respectively, without taking into account the required mass of water (it can be taken from the fuel cell). Regarding costs, the almost irreversible character of the reactions can make this alternative non-viable for extensive application; but the availability of cheap Mg scraps from the automotive industries [1] constitute an abundant vein of raw material that could be used for small portable applications. However, though reactions (1) and (2) are thermodynamically favorable, they are hampered because of the formation of a $MgO/Mg(OH)_2$ passive layer around the material that hinders the contact between the unreacted material and water, and considerably slows down the hydrolysis reaction at room temperature [2, 3].

Several alternatives have been proposed to avoid this problem [3-37], namely, 1) the acidification of the reaction environment, 2) the use of salt solutions, 3) the modification of the morphology to obtain nanostructured hydrolyzable materials, and 4) the incorporation of additives with different functions. The acidification of the solution dissolves the passive layer [4-9] and gives a fast and complete hydrolysis reaction, but the use of acid solutions presents important practical problems concerning reactor corrosion and potential hazards for users. The utilization of salt solutions, in particular chlorides solutions, has beneficial effects caused by Cl^- anions that strongly induce pitting corrosion [3, 10, 11]. A vast majority of papers reporting hydrogen production by hydrolysis use these solutions in the experiments [8, 9, 12-27] or hydrolyze a mixture of Mg or MgH_2 with a chloride salt prepared by mechanical milling [28-31]. Among the different chloride solutions those with Mg^{2+} and those with acidic cations like Zr^{4+}, Fe^{3+} and Ti^{3+} stand out for being more active [3, 31]. The effect of the acidic cations is well understood, but the reasons behind the Mg^{2+} effect are not clearly identified yet. Tegel et al. [31] have proposed that the formation of $MgCl_2{\cdot}3MgO{\cdot}11H_2O$ solid species could play a role during MgH_2 hydrolysis, and Chen et al. [14] have suggested that Mg^{2+} cations could capture some of the hydroxyls (OH^-) produced during the hydrolysis reaction and in this way reduce the formation of the $Mg(OH)_2$ layer. The third option to decrease the effect of the passive layer is nanostructuring the hydrolyzable material. This is mainly a physical way to minimize the effect of the passive layer. On one hand, the shorter the characteristic dimension of the material, the thinner the passive layer that has to be broken through to fully hydrolyze the material. On the other hand, the higher the specific surface, the faster the reaction rate and the greater the yield. A widely used technique to nanostructure materials is mechanical milling [8, 15, 16, 18-37]. The combination of cold welding and fracture produces homogeneous materials with small particles, high specific surface area and a microstructure that favors the hydrolysis reaction [37]. It is interesting to distinguish here the effects of milling MgH_2 or Mg. The brittle character of the first and the ductility of the second produce materials with different properties. By milling MgH_2 a few hours, nanometric powders that readily hydrolyze can be synthesized [8, 28, 31-34]. On the contrary, the ductility of Mg favors the cold welding process during milling and makes difficult to reduce Mg particles size and to increase the specific surface area [15]. This disadvantage can be partially avoided by the use of process-control agents such as graphite or carbon nanotubes during milling [21], but generally better results are achieved by milling MgH_2 than Mg. Other options to obtain nanostructured materials are plasma-metal reaction using Mg [9, 13, 14] or Mg + metal oxide [13]. The first has been used to produce a nanometric Mg [9] that exhibits a high total hydrogen production capacity of 910 mL/g, with fast kinetics (50% of reaction completion in just 0.4 min). The hydride prepared from these Mg

nanoparticles has also excellent hydrolysis properties, with a total production of 1770 mL/g and 50% of the reaction reached in 3.7 min [14]. The incorporation of additives to MgH_2 or Mg (usually by mechanical milling) promotes hydrolysis by different routes. For example, Ca, CaH_2, Li or $LiAlH_4$ react vigorously with water and when mixed with MgH_2 open up the MgH_2 structure and expose fresh surface to the solution improving hydrolysis [32, 33]. Transition metals such as Ni, Fe or Co and alloys of the Mg-Ni, Mg-Cu, Mg-Co systems promote galvanic corrosion and, in some cases, also improve particle comminution during milling [15, 16, 19-23, 27]. Metal oxides such as MoO_3, Fe_3O_4, Fe_2O_3, Nb_2O_5 and V_2O_5 also have a beneficial effect during hydrolysis [21, 24]. Finally, the incorporation of salts during milling has the double benefit of facilitating comminution during milling and producing a saline aqueous solution during the hydrolysis reaction [27-31].

In this work we report the synthesis, characterization and hydrolysis properties of two nanostructured materials: MgH_2 milled under hydrogen atmosphere and Mg obtained by dehydriding the as-milled MgH_2. The hydride presents average hydrolysis properties, with good yield and reasonable kinetics, and the Mg shows excellent hydrolysis properties with a high yield, fast kinetics and practically no passivating layer. These characteristics are associated with the morphology and microstructure of the material. By using this simple synthesis technique, the advantages of milling brittle MgH_2 are kept and the difficulties associated with milling ductile Mg are avoided. Effectively, part of the microstructural characteristics of the as-milled MgH_2 is retained after dehydriding, and we show that they have an impact on the hydrolysis.

2 Experimental details

Magnesium hydride powder (Sigma-Aldrich, 96.5%) was milled 5 h in a Fritsch Monomill Pulverisette P6 under 5 bar H_2 (99.999%) with a ball-to-powder mass ratio of 40:1 at room temperature. Milling was done under hydrogen to hydride residual Mg contained in the commercial material. To prevent overheating the milling schedule consisted of sequences of 10 min of milling followed by 15 min of pause. After this, a fraction of the milled MgH_2 was dehydrided at 355°C under vacuum for 2.5 h. During synthesis, all the materials were handled inside an Ar-filled glove box (UNILab MBraun, $O_2 < 1$ ppm and $H_2O < 1$ ppm) to prevent air exposure. The as-milled and dehydrided materials are designated as S-MgH_2 and S-Mg, respectively.

Crystallographic information was obtained by XRD using a Bruker Advance D8 diffractometer with Cu Kα radiation. The crystalline phases were identified by using the ICDD database and quantified by Rietveld refinement with TOPAS software [38]. Morphological analysis was performed on a SEM microscope (SEM-FIB Zeiss Crossbeam 340) and BET area was measured using a Micromeritics ASAP 2020 analyzer. In the last case the N_2 adsorption and desorption isotherms were acquired after cleaning the surface in vacuum at 100 °C overnight. Surface areas were determined by applying the Brunauer-Emmet-Teller (BET) model.

The hydrolysis experiments were carried out in a custom-made apparatus (Fig. 1) that is a modification of the experimental setup presented in [8]. The reaction occurs inside a Büchner flask. The flask is immersed in a circulating water bath to control reaction temperature, and put over a magnetic stirrer to agitate the reactants. Its mouth is connected to an Ar port and a bulb pipette, and its side arm is joined by a hose to a vertically placed burette. Additionally, a syringe for acid addition is mounted in the stopper of the Büchner flask. The burette is partially immersed into the water contained in a beaker put over a digital balance. Before the hydrolysis reaction, the sample is loaded inside the

Büchner flask on a custom-made ferromagnetic sample holder that is held in place by an external magnet. The sequence of the experiment is the following. After loading the sample in the Ar-purged system, some of the water contained in the beaker is suctioned with the bulb pipette to fill the burette. Then, the valve that connects the flask with the Ar port and the bulb pipette is closed and the reaction is initiated by removing the external magnet and letting the sample fall into the solution. As the reaction proceeds, the released H_2 displaces the water in the burette thus increasing the amount of water contained in the beaker. This increase is registered by the balance and automatically acquired by a PC. After 1 h of reaction 10 mL of 0.5 M HCl are added to the solution to dissolve the passive layer and completely hydrolyze the sample. In the experiments S-MgH_2 and S-Mg samples of approximately 30 mg were hydrolyzed in 50 mL of a 0.6 M $MgCl_2$ solution. All the samples were exposed to atmospheric air for approximately 7 min before being introduced into the flask (variation of the exposure time between 2 and 12 minutes did not produce appreciable changes in the hydrolysis reaction). The combination of the thermal bath and the low sample/solution ratio resulted in practically isothermal hydrolysis reactions. As an example, Fig. S1 in the supplementary material shows a maximal temperature increase of 1 K during the hydrolysis of 39.8 mg of S-Mg at room temperature. The errors in the amount of hydrogen released were estimated at 3% for the hydrolysis in solution and 6% after the addition of acid.

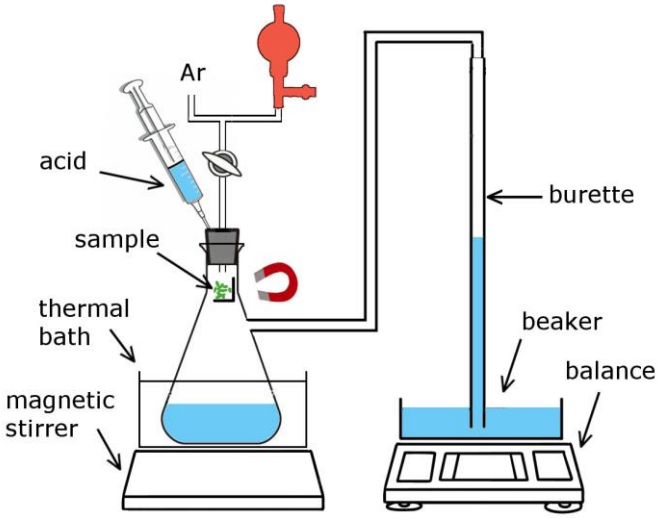

Figure 1. Diagram of the hydrolyzer.

3 Results and discussion

The XRD of S-MgH_2 (Fig. 2) shows peaks that correspond to β-MgH_2 (PDF 00-012-0697), γ-MgH_2 (PDF 00-035-1184) and a small contribution from MgO (PDF 00-045-0946). The β polymorph, which is the main component of the starting material, is the most abundant phase after 5 h of milling, as it can be seen in Table 1, that contains the quantification obtained after Rietveld refinement of the data. The metastable γ polymorph is typically observed in milled materials [39] and the small amount of MgO is a consequence of residual oxygen content and air exposure during XRD measurement. All phases exhibit broad peaks because milling reduces crystallite size, produces microstrain and introduces defects in the lattice. After dehydriding at 355 °C to obtain S-Mg both MgH_2-polymorphs decompose into Mg (PDF 00-035-0821) as it can be seen in the corresponding diffractogram (Fig. 2). Additionally, a slightly higher amount of MgO (7 wt.%) is estimated from Rietveld quantification (Table 1). Mg peaks

are significantly thinner than MgH_2 peaks due to crystallites growth and defects reduction during dehydriding.

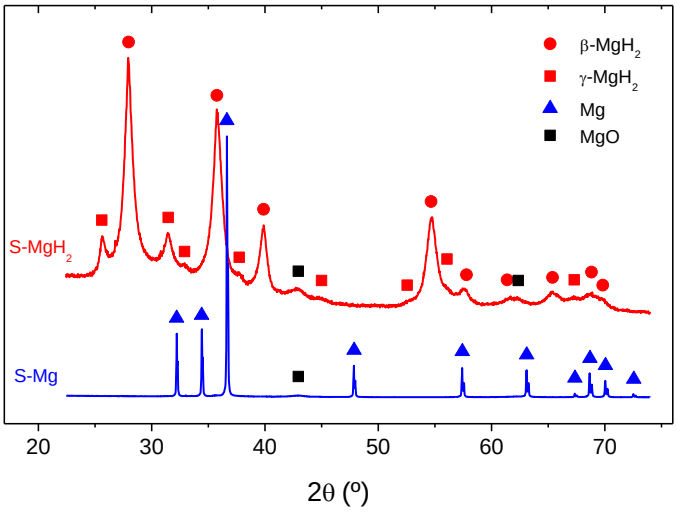

Figure 2. XRD of the material as-milled (S-MgH_2) and after dehydriding (S-Mg).

	Quantification (wt.%)				Crystallite size (nm)			Quality	
	Mg	β-MgH_2	γ-MgH_2	MgO	Mg	β-MgH_2	γ-MgH_2	R_{wp}	χ^2
S-MgH_2	--	60(3)[a]	36(4)	4(2)	--	7	6	3.9	1.8
S-Mg	93(2)	--	--	7(2)	250	--	--	7.8	3.5

[a] The figures within parentheses stand for the error.

Table 1. Phase abundance in S-MgH_2 and S-Mg from Rietveld refinement of the diffractograms of Fig. 2.

Mechanical milling also affects morphology and particle size distribution. Milling comminutes the commercial MgH_2 (150-200 μm, not shown here) into small particles (Fig. 3 a and c). The prevailing morphology of S-MgH_2 consists of agglomerates with a wide range of sizes, from 5 to 100 μm, that seem to be composed of particles with typical sizes of the order of 10 nm. The BET specific surface area of this material is 9 m^2/g, in agreement with previously reported values for MgH_2 milled without additives and in agreement with the morphology observed here by SEM [15, 34]. The morphology of S-Mg at the micrometer scale is similar to that of S-MgH_2 (Fig. 3b). However, at the nanometer scale, different and varied morphologies are observed (Fig. 3d, e and f). In some cases (Fig. 3d) the particles that form the agglomerates have similar sizes to those of S-MgH_2, of the order of 10 nm, but gathering to form a rougher surface. In other cases (Fig. 3e), the agglomerates have smoother surfaces, where particles of approximately 100 nm can be individualized. These agglomerates exhibit also rod-like structures of approximately 100 nm long by 10 nm wide. Finally, Fig. 3f, shows compact hexagonal faceted crystals with sizes of the order of 100 nm. These morphologies have also been observed in vapor-deposited Mg materials [40], and the formation and abundance of each one depend on the experimental conditions. It seems that during dehydriding, part of the Mg formed at the first stages of the process evaporates and subsequently deposits in other regions of the sample forming the aforementioned structures. As a consequence of this, and the microstructure of the parent S-MgH_2, the complex, rather inhomogeneous morphology of S-Mg arises. The BET surface area of S-Mg, 13

m^2/g, is slightly larger than the value obtained for S-MgH_2 and one order of magnitude larger than the value 1 m^2/g reported for Mg mechanically milled without additives [15].

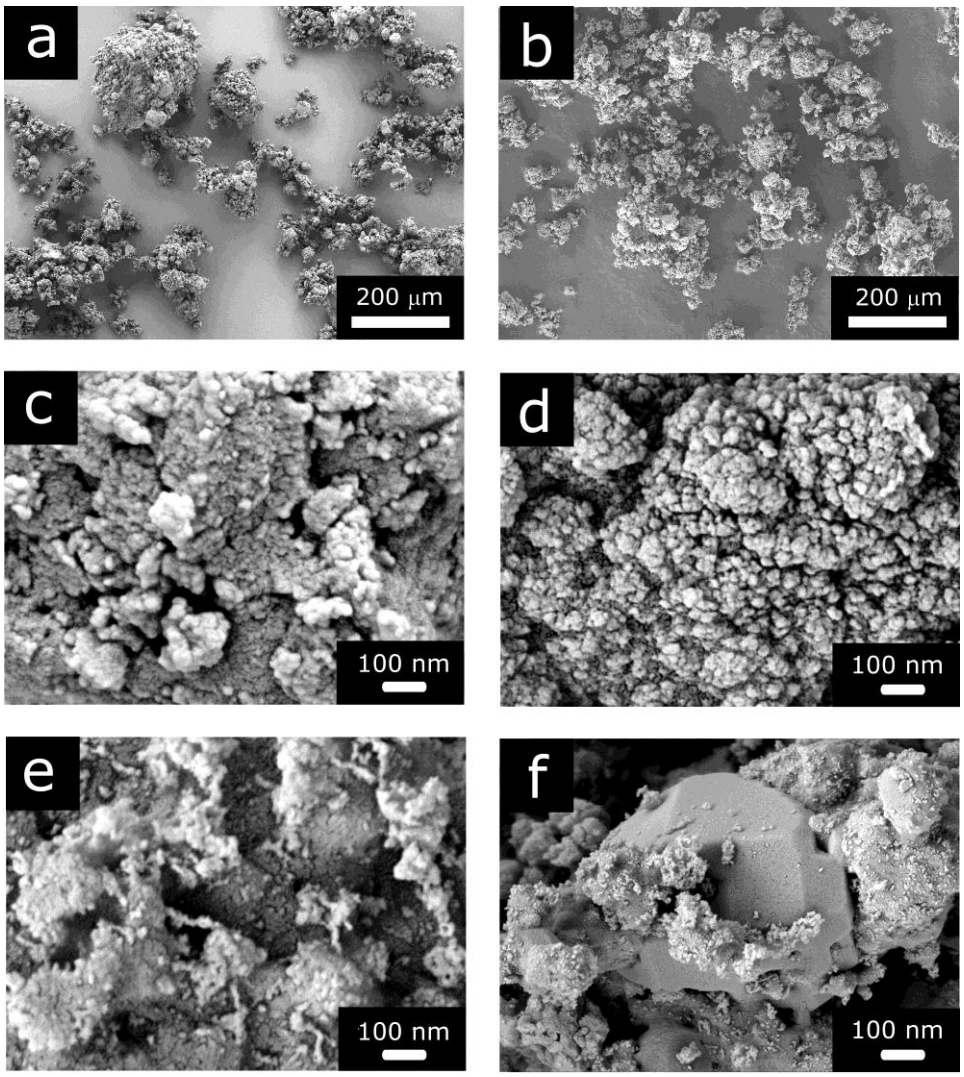

Figure 3. SEM micrographs corresponding to S-MgH_2 (a,c) and S-Mg (b, d-f).

The hydrolysis of S-MgH_2 near ambient temperature (24 °C) proceeded straightforwardly without induction time, as is shown in Fig. 4. After 1 h of reaction, 1390 mL/g of H_2 was produced. After this, by adding hydrochloric acid to the solution, an additional amount of H_2 was released giving a hydrogen production of 1670 mL/g. This extra hydrogen was produced as a consequence of the dissolution of the passive layer by the acid. The difference between this value and the expected amount of hydrogen released by MgH_2, 1880 mL/g, is due to the presence of MgO in the material.

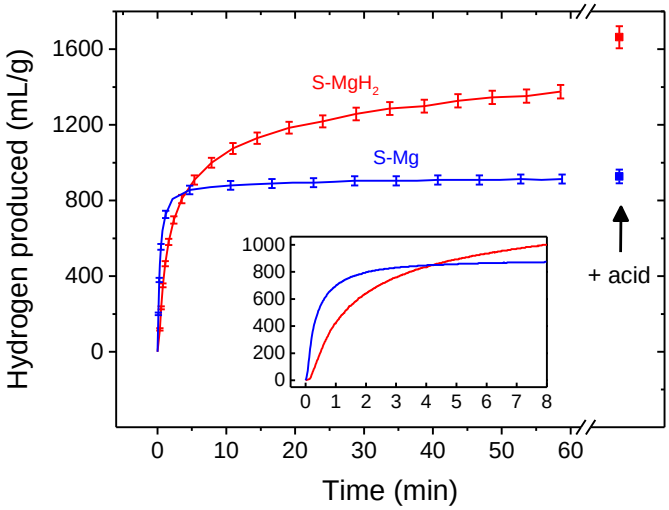

Figure 4. Hydrogen released by S-Mg and S-MgH_2 at room temperature (24 °C). The amount of hydrogen produced after acid incorporation is indicated by the arrow.

The comparison of the hydrolysis performance of S-MgH_2 with that of different MgH_2 based materials, with and without additives, can be made with the help of Table 2. Beginning with the materials without additives it can be seen that only the MgH_2 prepared by hydrogen plasma metal reaction followed by hydriding made by Chen et al. [14], and the MgH_2 obtained by hydriding 200-mesh Mg [12] have hydrolysis performances in terms of yield and kinetics better than that of S-MgH_2. In the first case the better performance can be attributed to the microstructure of nano MgH_2 and the concentration of the $MgCl_2$ solution used. In the second case, the higher yield can be linked with the microstructure and with the use of a solution with the acidic Al^{3+} cation. The other results reported in the literature for MgH_2 without additives have either lower yield or slower kinetics [8, 13, 15, 31-34]. In some cases, the differences could be due to the solution concentration [8, 13], the solution type [15], or the use of distilled water [31-34]. The comparison with the MgH_2 with additives materials reported in the literature exhibiting the best results [13, 16, 31], shows that they have higher capacities but similar or slower kinetics. The variety of synthesis techniques and additives makes difficult to identify the particular causes for the higher capacities, but it is interesting to remark that all of them use chloride solutions or have been prepared by milling with chlorides (three of them with $MgCl_2$).

Material	Additive	Morphology	Hydrolysis solution	Reaction temp. (°C)	Total H_2 produced (mL/g)	Total reaction time (min)	Time for 50% of max. capacity (min)	Activation energy (kJ/mol)	Ref.
Mg prepared by hydrogen plasma metal reaction + hydriding	-	powder avg part. size 0.8 µm	1 M $MgCl_2$	25	1770	20	3.7	-	[14]
200-mesh Mg + hydriding	-	powder	0.5 M $AlCl_3$	30	1690	20	2.5	22	[12]
MgH_2 prepared by hydrogen plasma metal reaction + hydriding	-	powder avg part. size 0.9 µm	0.1 M $MgCl_2$	25	1167	60	8.1	53	[13]
MgH_2 milled 3 h in H_2 (QM-3SP4)	-	powder	0.05 M $MgCl_2$	25	1130	90	9.0	-	[8]
MgH_2 milled 0.5 h in Ar (Spex 8000)	-	powder avg part. size < 10 µm	1 M KCl	RT	660	60	4.9	-	[15]
MgH_2 milled 20 h in Ar (Spex 8000)	-	powder	water	-	1370	1200	172	-	[33]
MgH_2 milled 3 h in H_2 (Retsch PM100)	-	powder	water	RT	580	23	2.4	-	[34]
MgH_2 milled 1 h in Ar (P6)	-	powder median part. size 3-8 µm	water	22	470	50	2.8	-	[31]
MgH_2 milled 10 h in Ar (Spex 8000)	-	powder	water	-	300	20	~1	-	[32]
S-MgH_2: MgH_2 milled 5 h in H_2 (P6)	-	powder agglomerates 5-100 µm, particles ~10 nm	0.6 M $MgCl_2$	24	1390	60	2.3	37	(this work)
MgH_2 + 1 mol.% Ni mixture hydrided and milled 1 h in Ar	1 mol.% Ni	powder	0.5 M $MgCl_2$	30	1640	30	2.4	-	[16]
MgH_2 + 2.4 mol.% $ZrCl_4$ milled 1 h in Ar (P6)	2.4 mol.% $ZrCl_4$	powder median part. size 3-8 µm	water	22	1460*	70	3.9	-	[31]
MgH_2 + 2.4 mol.% $MgCl_2$ milled 1 h in Ar (P6)	2.4 mol.% $MgCl_2$	powder median part. size 3-8 µm	water	22	1550*	70	8.4	-	[31]
MgH_2 prepared by arc plasma + 10 wt.% TiO_2 + H_2 activation	10 wt.% TiO_2	powder avg part. size 1 µm	0.1 M $MgCl_2$	25	1520	40	8.1	45	[13]

RT: room temperature as referred in the cited reference.
* These values were estimated assuming that samples complete the reaction after the addition of acid.

Table 2. Hydrolysis properties at ambient temperature of selected MgH_2-based materials reported in the literature.

The hydrolysis of S-Mg at room temperature (Fig. 4) did not present an induction time either, and after 1 h it released 910 mL/g of H_2. When acid was added to the solution, a small amount of extra H_2 was produced, totaling 920 mL/g. This result suggests that practically no hydrolyzable Mg is lost as a

consequence of the passivating layer. As in the case of S-MgH_2, the presence of MgO in the material accounts for the difference between the hydrogen produced after the addition of acid and the amount of hydrogen expected from pure Mg (1020 mL/g).

The hydrolysis performance of some Mg-based materials reported in the literature is compiled in Table 3. Among the materials prepared without additives, the only material with better capacity and kinetics is the Mg prepared by hydrogen plasma metal reaction by Zheng et al. [9] when hydrolyzed in a 0.1 M $AlCl_3$ solution. If the same material is hydrolyzed in a 0.5 M $MgCl_2$ solution the performance is similar to that of S-Mg, pointing out the relevance of the hydrolysis solution. The Mg prepared by vapor deposition by Liu et al. [17] exhibits hydrolysis performance slightly below that of S-Mg, and the materials prepared by mechanical milling (without additives) [15, 18-20] also exhibit capacities and kinetics below that of S-Mg. These results show how difficult it is to nanostructure pure Mg by mechanical milling under Ar. The Mg-based materials made by using additives and showing the best hydrolysis properties, to the best of our knowledge, are those reported in [21-23]. It is interesting to note that despite the use of different additives their hydrolysis performance is not better than that of S-Mg, though it has to be taken into consideration that all of them use NaCl solutions instead of the more reactive $MgCl_2$ solutions.

Material	Additive	Morphology	Hydrolysis solution	Reaction temp. (°C)	Total reaction time (min)	Total H_2 produced (mL/g)	Time for 50% of max. capacity (min)	Activation energy	Ref.
Mg prepared by hydrogen plasma metal reaction	-	powder avg. part. size 0.5 µm	0.1 M $AlCl_3$	RT	25	935	~0.1	-	[9]
Mg prepared by hydrogen plasma metal reaction	-	powder avg. part. size 0.5 µm	0.5 M $MgCl_2$	RT	60	910	1.6	-	[9]
Mg prepared by vapor deposition	-	cell-like nanoporous Mg	1.8 M NaCl	25	15	808	3.8	-	[17]
Mg milled 0.5 h in Ar (SPEX 8000)	-	platelets avg. size > 100 µm	1 M KCl	RT	60	860	13.7	-	[15]
Mg milled 1 h in Ar (QM-3SP4)	-	powder	seawater	25	300	805	65	64	[18]
Mg milled 1 min in Ar (AGO-2U type)	-	powder avg. part. size 170 µm	0.9 M NaCl	21-23	120	755	32	-	[19]
Mg milled 3 min in Ar (AGO-2U type)	-	powder	0.032 M $NiCl_2$	-	-	663	0.8	-	[20]
Mg milled 3 min in Ar (AGO-2U type)	-	powder	0.85 M NaCl	-	-	499	6.8	-	[20]
S-Mg: MgH_2 milled 5 h in H_2 (P6) + dehydriding	-	powder with varied morphology (see above)	0.6 M $MgCl_2$	24	15	910	0.3	18	(this work)
Mg + 5 wt.% graphite + 5 wt.% Ni milled 1 h in H_2 (P5)	5 wt.% graphite + 5 wt.% Ni	powder	0.6 M NaCl	25	3.3	910	0.4	14	[21]
Mg + 10 wt.% graphite milled 5 h in H_2 (P5)	10 wt.% graphite	powder avg. part. size 110 µm	0.6 M NaCl	25	8.3	910	0.6	18	[21]
Mg + 10 wt. % nano MoS_2 milled 1 h in Ar (QM-3SP4)	10 wt. % nano MoS_2	powder	0.6 M NaCl	25	0.6	845	0.02	13	[22]
Mg + 10 wt.% In milled 1 h in Ar (Simoloyer CM01)	10 wt.% In	powder	seawater	30-55	10	855	1.0	12	[23]
RT: room temperature as referred in the cited reference.									

Table 3. Hydrolysis properties at ambient temperature of selected Mg-based materials reported in the literature.

Comparing now the hydrolysis performance of S-MgH_2 and S-Mg it is difficult to reach a conclusive statement. Though the hydrogen production capacity of S-MgH_2 (1390 mL/g) is higher than that of S-Mg (910 mL/g), S-Mg is much more reactive. Its hydrolysis curve reached 50% of the full capacity in

0.3 min and 90% in 2.6 min, whereas S-MgH_2 reached 50% in 2.3 min, and did not attain completion after 1 h.

To explore if the high reactivity of S-Mg and the high yield of S-MgH_2 can be combined into a single material, a partially dehydrided MgH_2 has been prepared. To this end the as-milled MgH_2 was dehydrided under vacuum at 355 °C for 7 min instead of 2.5 h. After this, the material presented 45 wt. % of β-MgH_2, 48 wt. % of Mg and 7 wt. % of MgO as determined from Rietveld refinement of XRD data (see Fig. S2 and Table S1, Supplementary Material). Fig. 5 shows the hydrolysis curve of this material at 24 °C. For comparison, a hydrolysis curve made by the linear combination of the S-Mg and S-MgH_2 curves in the proportions given by the abundance of each phase in the material is also shown. This last curve can be taken as the expected hydrolysis curve if S-Mg and S-MgH_2 had kept their individual hydrolysis properties in the partially dehydrided material. It can be seen that the experimental curve lies most of the time slightly below the expected curve, reaching the expected capacity after 1 h. After acid addition, the hydrogen released increases to 1300 mL/g, the value expected from the phase abundances determined from Rietveld refinement. Therefore, the hydrolysis performance of the partially dehydrided sample does not exceed that of S-Mg or S-MgH_2 neither from the kinetics nor the hydrogen production points of view. The reasons behind this behavior are not fully understood yet, but the complex morphology of a partially dehydrided material, the distribution and location of Mg and β-MgH_2 in the material and the simultaneous occurrence of reactions (1) and (2) can be mentioned as potential factors that could affect the hydrolysis process.

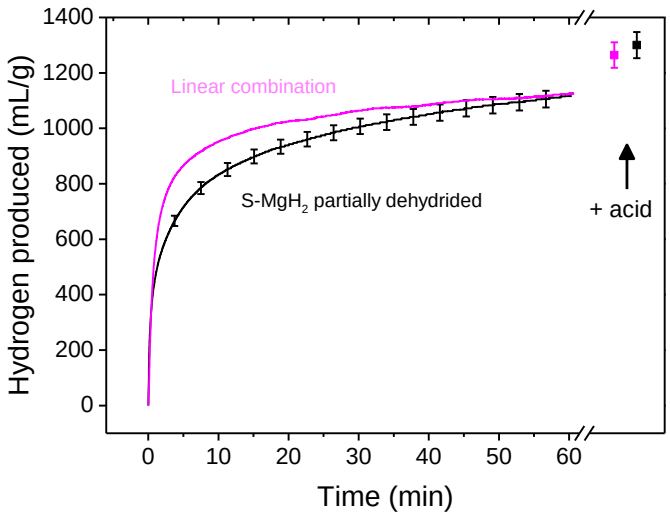

Figure 5. Hydrogen released at room temperature (24 °C) by S-MgH_2 partially dehydrided (black) and theoretical curve obtained by linear combination of the hydrogen released by S-MgH_2 and S-Mg (magenta, see text). The amount of hydrogen produced after acid incorporation is indicated by the arrow.

Figs. 6 and 7 present the hydrolysis curves of S-MgH_2 and S-Mg at different temperatures from 10 °C to 50 °C. Kinetics increases with temperature, as expected, and hydrogen production capacity after acid addition coincide within experimental errors for all materials (Table 4).

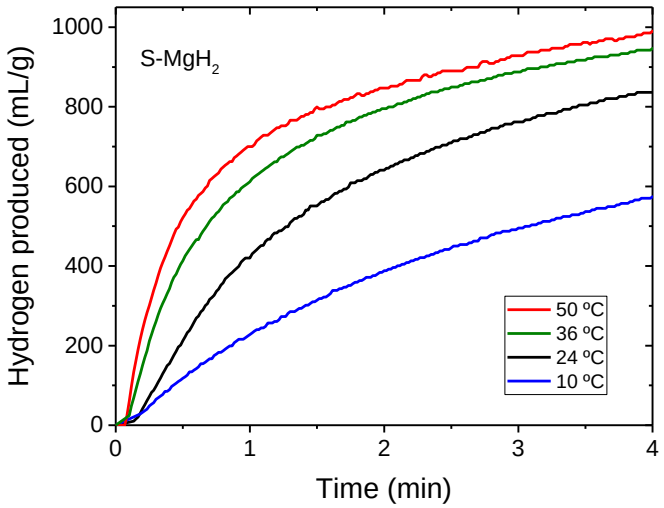

Figure 6. Hydrogen released by S-MgH_2 at different temperatures.

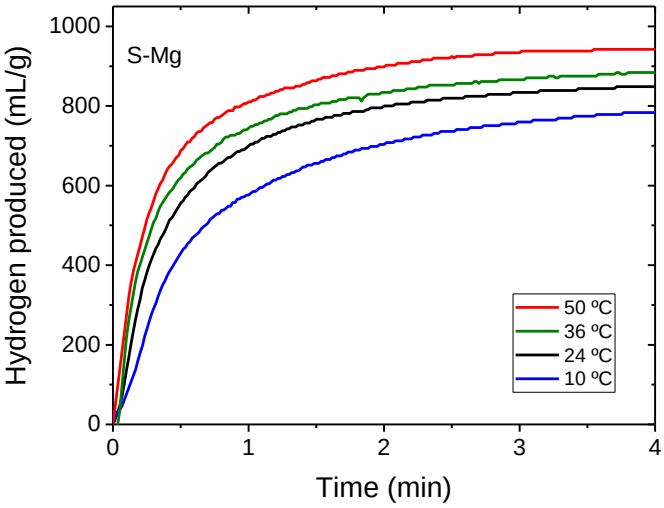

Figure 7. Hydrogen released by S-Mg at different temperatures.

	Temperature (°C)	H_2 produced (mL/g)	H_2 produced after acid addition (mL/g)
S-MgH_2	10	1170(40)[a]	1570(60)
	24	1390(40)	1670(60)
	36	1360(40)	1630(70)
	50	1500(40)	1680(70)
S-Mg	10	880(20)	890(50)
	24	910(20)	920(40)
	36	920(20)	940(40)
	50	960(20)	940(50)

[a] The figures within parentheses stand for the error.

Table 4. Yield obtained for the reaction of S-MgH_2 and S-Mg with the saline solution and after acid addition at different temperatures.

From the hydrolysis curves at different temperatures the apparent activation energies were estimated by the slope of the linear fit of the Arrhenius plot of $\ln \frac{d\alpha}{dt}$ vs. 1/T (Fig. 8), where $\frac{d\alpha}{dt}$ is taken at α=0.3 (α being the conversion fraction).

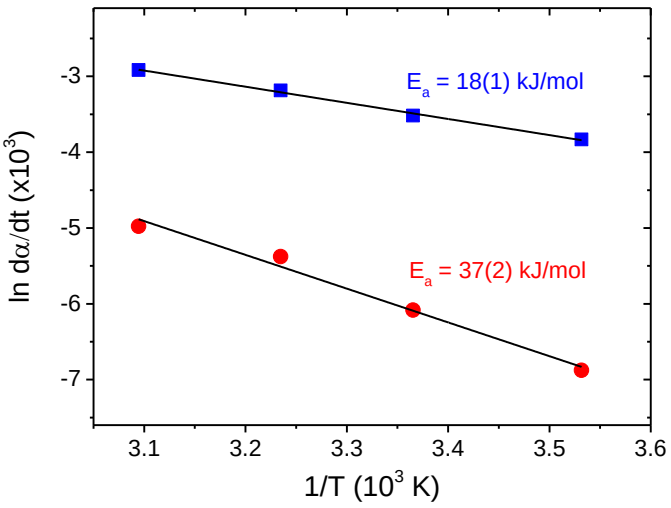

Figure 8. Arrhenius plot using the rates obtained from Figs. 6 (red circles) and 7 (blue squares) that correspond to S-MgH_2 and S-Mg, respectively.

By following this procedure, activation energies of 37 kJ/mol for S-MgH_2 and 18 kJ/mol for S-Mg were determined. These activation energies correlate with the kinetic behavior showed by the materials. Comparing with literature results it can be observed that in the case of MgH_2 there is some dispersion in activation energies (Table 2). The value obtained for S-MgH_2 is more or less in the middle of the range spanned by the literature values (22-53 kJ/mol). In the case of Mg, the reported activation energies can be classified according to the use or not of additives. In the first case, several values covering the range between 12 and 18 kJ/mol have been reported [21, 22, 23]. In the second case, only the 64 kJ/mol value given in Ref. [18] could be found. The value reported here of 18 kJ/mol (no additives) is considerably smaller than that of Ref. [18], and lies in the upper limit of the range spanned by the materials prepared with additives. A possible explanation for this fact is that the combination of milling brittle MgH_2 and dehydriding is much more effective to obtain an alternative hydrolysis path than milling ductile Mg under Ar (Ref. [18]).

From the point of view of mechanism, the hydrolysis reactions of S-Mg and S-MgH_2 are different. The main reason for this is that in the first case hydrogen comes from water, and the electrons to reduce this hydrogen come from Mg that oxidizes to Mg^{2+}. In the second case hydrogen comes from both water and MgH_2, and hydride ions provide the electrons to reduce water protons. Going into details, the corrosion of Mg in neutral or alkaline aqueous solution occurs in several steps [41, 42]. The first one involves the cleavage of a water molecule, the adsorption of a H atom on the metal surface and the release of a hydroxyl ion (Volmer step)

Volmer step: $Mg + H_2O \rightarrow [Mg\text{-}H^{ad}]^+ + OH^-$ (3)

Then, two pathways can be followed: in the first one a hydrogen molecule is released via the interaction of an H^{ad} and a water molecule (Heyrovsky step), or in the second one, H_2 is released by the combination of two H^{ad} (Tafel step). In both cases one Mg^{2+} ion is released in the global process.

Heyrovsky step: $H_2O + [Mg\text{-}H^{ad}]^+ \rightarrow H_2 + OH^- + Mg^{2+}$ (4)

Tafel step: $[Mg\text{-}H^{ad}]^+ + [Mg\text{-}H^{ad}]^+ \rightarrow H_2 + Mg^{2+} + Mg$ (5)

Both processes could simultaneously occur in neutral aqueous solution, whereas the Heyrovsky step is the preferred pathway when corrosion of Mg is produced in alkaline media [41]. In the case of the S-Mg hydrolysis experiments the solution becomes alkaline due to the reaction itself (see Eq. 1).

The elementary steps involved in the hydrolysis mechanism of MgH_2 are not as studied as those of the hydrolysis of Mg. Recently, Chen et al. [14] have proposed a mechanism for the hydrolysis of MgH_2 in deionized water that could be decomposed in the following elementary steps. In the first stage, by the cleavage of two water molecules a $[H^+\text{-}H^{\delta-}Mg^{2\delta+}H^{\delta-}\text{-}H^+]^{2+}$ intermediate species and two hydroxyl ions are produced.

$H^{\delta-}Mg^{2\delta+}H^{\delta-} + 2H_2O \rightarrow [H^+\text{-}H^{\delta-}Mg^{2\delta+}H^{\delta-}\text{-}H^+]^{2+} + 2OH^-$ (6)

In a second step, from the interaction between H^+, $H^{\delta-}$ and $Mg^{2\delta+}$, two H_2 molecules are released and one Mg^{2+} ion is produced

$[H^+\text{-}H^{\delta-}Mg^{2\delta+}H^{\delta-}\text{-}H^+]^{2+} \rightarrow 2\,H_2 + Mg^{2+}$ (7)

In a later step the Mg^{2+} cation could react with the hydroxyl ions to form $Mg(OH)_2$. Eventually, the formation of the intermediate $[H^+\text{-}H^{\delta-}Mg^{2\delta+}H^{\delta-}\text{-}H^+]^{2+}$ could occur in two sequential steps as detailed below:

$H^{\delta-}Mg^{2\delta+}H^{\delta-} + H_2O \rightarrow [H^{\delta-}Mg^{2\delta+}H^{\delta-}\text{-}H^+]^+ + OH^-$ (8)

$[H^{\delta-}Mg^{2\delta+}H^{\delta-}\text{-}H^+]^+ + H_2O \rightarrow [H^+\text{-}H^{\delta-}Mg^{2\delta+}H^{\delta-}\text{-}H^+]^{2+} + OH^-$ (9)

The point is that the elementary steps during the hydrolysis of Mg or MgH_2 are not the same. The main reason behind this is that Mg has to oxidize to Mg^{2+} to provide the electrons to reduce hydrogen during the hydrolysis of Mg whereas it is already in the Mg^{2+} form in MgH_2, whose hydride species provide the electrons and half of the hydrogen atoms that are released. As a consequence, the activation energies for each process are not directly comparable.

Summarizing, by milling MgH_2 without additives we obtained a material that can produce hydrogen in a 0.6 M $MgCl_2$ solution with hydrolysis properties as good as those of the best materials reported in the literature. Additionally, by dehydriding the as-milled MgH_2 we have obtained a nanometric Mg powder with a microstructure and specific surface area closer to that of milled MgH_2, instead of that obtained when milling ductile Mg. The properties of this Mg make possible to produce hydrogen in a $MgCl_2$ solution with optimal kinetics and a higher yield. Additionally, it is worth to mention that these hydrolysis properties are observed despite the recrystallization and coalescence observed on the diffractogram (Fig. 2) and some S-Mg micrographies (Fig. 3) consequence of the dehydriding process at 355 °C. The results reported here lead to the possibility of applying this synthesis procedure to other metals whose ductility prevents an optimum nanostructuring by mechanical milling.

4 Conclusions

A nanometric Mg with excellent hydrolysis properties has been synthesized by combining mechanical milling and dehydriding. This material produces 910 mL/g of H_2 in a 0.6 M $MgCl_2$ aqueous solution, releasing 50% of the hydrogen in 0.3 min and 90% of it in 2.6 min. This hydrolysis performance is among the bests reported in the literature for Mg-based materials, and is attributed to the morphology and microstructure of the material. By mechanical milling MgH_2 followed by dehydriding a finely comminuted Mg powder with high specific surface area is obtained. Effectively, this combined technique allows to avoid the difficulties associated with the mechanical milling of ductile Mg. The parent material, the as-milled MgH_2, also has very good hydrolysis properties, producing 1390 mL/g of H_2 in 1 hour, but with slower kinetics. The apparent activation energies of these reactions have been estimated from hydrolysis experiments at different temperatures. In the S-Mg case an activation energy of 18 kJ/mol has been determined, while in the S-MgH_2 case a value of 37 kJ/mol has been obtained. These activation energies correlate with the kinetic performance of the materials, and the obtained values are within the ranges reported in the literature.

Acknowledgments

This work was partially supported by grants from CONICET [PIP 112 201501 00610]; SGCTeYP-ECOS SUD [A17A03]; and Universidad Nacional de Cuyo [06/C602].

References

[1] Hanko G, Antrekowitsch H, Ebner P. Recycling automotive magnesium scrap. JOM Journal of the Minerals, Metals and Materials Society. 2002;54(2):51–54. https://doi.org/10.1007/BF02701075

[2] Esmaily M, Svensson JE, Fajardo S, Birbilis N, Frankel GS, Virtanen S, et al. Fundamentals and advances in magnesium alloy corrosion. Progress in Materials Science. 2017 Aug;89:92–193. https://doi.org/10.1016/j.pmatsci.2017.04.011

[3] Corrosion Resistance of Aluminum and Magnesium Alloys Understanding, Performance and Testing. Corrosion Engineering, Science and Technology. 2011 Feb;46(1):1–2. https://doi.org/10.1179/147842211X12948245627839

[4] Uan J-Y, Yu S-H, Lin M-C, Chen L-F, Lin H-I. Evolution of hydrogen from magnesium alloy scraps in citric acid-added seawater without catalyst. International Journal of Hydrogen Energy. 2009 Aug 1;34(15):6137–42. https://doi.org/10.1016%2Fj.ijhydene.2009.05.133

[5] Hiraki T, Hiroi S, Akashi T, Okinaka N, Akiyama T. Chemical equilibrium analysis for hydrolysis of magnesium hydride to generate hydrogen. International Journal of Hydrogen Energy. 2012 Sep 1;37(17):12114–9. https://doi.org/10.1016/j.ijhydene.2012.06.012

[6] Kojima Y, Suzuki K-I, Kawai Y. Hydrogen generation by hydrolysis reaction of magnesium hydride. Journal of Materials Science. 2004 Mar;39(6):2227–9. https://doi.org/10.1023/B:JMSC.0000017794.92899.bd

[7] Huang M, Ouyang L, Wang H, Liu J, Zhu M. Hydrogen generation by hydrolysis of MgH2 and enhanced kinetics performance of ammonium chloride introducing. International Journal of Hydrogen Energy. 2015 May 18;40(18):6145–50. https://doi.org/10.1016%2Fj.ijhydene.2015.03.058

[8] Ouyang L, Ma M, Huang M, Duan R, Wang H, Sun L, et al. Enhanced Hydrogen Generation Properties of MgH2-Based Hydrides by Breaking the Magnesium Hydroxide Passivation Layer. Energies. 2015 May;8(5):4237–52. https://doi.org/10.3390%2Fen8054237

[9] Zheng J, Yang D, Li W, Fu H, Li X. Promoting H2 generation from the reaction of Mg nanoparticles and water using cations. Chemical Communications. 2013;49(82):9437. https://doi.org/10.1039%2Fc3cc45021j

[10] Makar GL. Corrosion Studies of Rapidly Solidified Magnesium Alloys. J Electrochem Soc. 1990;137(2):414. https://doi.org/10.1149/1.2086455

[11] Song GL, Atrens A. Corrosion Mechanisms of Magnesium Alloys. Advanced Engineering Materials. 1999 Sep 1;1(1):11–33. https://doi.org/10.1002/(SICI)1527-2648(199909)1:1<11::AID-ADEM11>3.0.CO;2-N

[12] Gan D, Liu Y, Zhang J, Zhang Y, Cao C, Zhu Y, et al. Kinetic performance of hydrogen generation enhanced by AlCl3 via hydrolysis of MgH2 prepared by hydriding combustion synthesis. International Journal of Hydrogen Energy. 2018 May 31;43(22):10232–9. https://doi.org/10.1016/j.ijhydene.2018.04.119

[13] Yang B, Zou J, Huang T, Mao J, Zeng X, Ding W. Enhanced hydrogenation and hydrolysis properties of core-shell structured Mg-MOx (M = Al, Ti and Fe) nanocomposites prepared by arc plasma method. Chemical Engineering Journal. 2019 Sep 1;371:233–43. https://doi.org/10.1016%2Fj.cej.2019.04.046

[14] Chen J, Fu H, Xiong Y, Xu J, Zheng J, Li X. MgCl2 promoted hydrolysis of MgH2 nanoparticles for highly efficient H2 generation. Nano Energy. 2014 Nov;10:337–43. https://doi.org/10.1016%2Fj.nanoen.2014.10.002

[15] Grosjean M, Zidoune M, Roue L, Huot J. Hydrogen production via hydrolysis reaction from ball-milled Mg-based materials. International Journal of Hydrogen Energy. 2006 Jan;31(1):109–19. https://doi.org/10.1016%2Fj.ijhydene.2005.01.001

[16] Zhao Z, Zhu Y, Li L. Efficient catalysis by MgCl2 in hydrogen generation via hydrolysis of Mg-based hydride prepared by hydriding combustion synthesis. Chemical Communications. 2012;48(44):5509. https://doi.org/10.1039%2Fc2cc32353b

[17] Liu J, Wang H, Yuan Q, Song X. A novel material of nanoporous magnesium for hydrogen generation with salt water. Journal of Power Sources. 2018 Aug;395:8–15. https://doi.org/10.1016/j.jpowsour.2018.05.062

[18] Huang M, Ouyang L, Ye J, Liu J, Yao X, Wang H, et al. Hydrogen generation via hydrolysis of magnesium with seawater using Mo, MoO2, MoO3 and MoS2 as catalysts. J Mater Chem A. 2017 May 10;5(18):8566–75. https://doi.org/10.1039/C7TA02457F

[19] Kravchenko OV, Sevastyanova LG, Urvanov SA, Bulychev BM. Formation of hydrogen from oxidation of Mg, Mg alloys and mixture with Ni, Co, Cu and Fe in aqueous salt solutions. International Journal of Hydrogen Energy. 2014 Apr;39(11):5522–7. https://doi.org/10.1016%2Fj.ijhydene.2014.01.181

[20] Sevastyanova LG, Genchel VK, Klyamkin SN, Larionova PA, Bulychev BM. Hydrogen generation by oxidation of "mechanical alloys" of magnesium with iron and copper in aqueous salt solutions. International Journal of Hydrogen Energy. 2017 Jul 6;42(27):16961–7. https://doi.org/10.1016%2Fj.ijhydene.2017.05.242

[21] Awad AS, El-Asmar E, Tayeh T, Mauvy F, Nakhl M, Zakhour M, et al. Effect of carbons (G and CFs), TM (Ni, Fe and Al) and oxides (Nb2O5 and V2O5) on hydrogen generation from ball milled Mg-based hydrolysis reaction for fuel cell. Energy. 2016 Jan;95:175–86. https://doi.org/10.1016%2Fj.energy.2015.12.004

[22] Huang M, Ouyang L, Liu J, Wang H, Shao H, Zhu M. Enhanced hydrogen generation by hydrolysis of Mg doped with flower-like MoS2 for fuel cell applications. Journal of Power Sources. 2017 Oct 15;365:273–81. https://doi.org/10.1016%2Fj.jpowsour.2017.08.097

[23] Xiao F, Guo Y, Yang R, Li J. Hydrogen generation from hydrolysis of activated magnesium/low-melting-point metals alloys. International Journal of Hydrogen Energy. 2019 Jan 15;44(3):1366–73. https://doi.org/10.1016%2Fj.ijhydene.2018.11.165

[24] Huang M, Ouyang L, Chen Z, Peng C, Zhu X, Zhu M. Hydrogen production via hydrolysis of Mg-oxide composites. International Journal of Hydrogen Energy. 2017 Aug 31;42(35):22305–11. https://doi.org/10.1016%2Fj.ijhydene.2016.12.099

[25] Alasmar E, Awad AS, Hachem D, Tayeh T, Nakhl M, Zakhour M, et al. Hydrogen generation from Nd-Ni-Mg system by hydrolysis reaction. Journal of Alloys and Compounds. 2018 Apr 5;740:52–60. https://doi.org/10.1016/j.jallcom.2017.12.305

[26] Tan Z, Ouyang L, Liu J, Wang H, Shao H, Zhu M. Hydrogen generation by hydrolysis of Mg-Mg2Si composite and enhanced kinetics performance from introducing of MgCl2 and Si. International Journal of Hydrogen Energy. 2018 Feb;43(5):2903–12. https://doi.org/10.1016/j.ijhydene.2017.12.163

[27] Buryakovskaya OA, Vlaskin MS, Ryzhkova SS. Hydrogen production properties of magnesium and magnesium-based materials at low temperatures in reaction with aqueous solutions. Journal of Alloys and Compounds. 2019 May 15;785:136–45. https://doi.org/10.1016%2Fj.jallcom.2019.01.003

[28] Grosjean M-H, Roué L. Hydrolysis of Mg–salt and MgH2–salt mixtures prepared by ball milling for hydrogen production. Journal of Alloys and Compounds. 2006 Jun;416(1–2):296–302. https://doi.org/10.1016%2Fj.jallcom.2005.09.008

[29] Liu Y, Wang X, Dong Z, Liu H, Li S, Ge H, et al. Hydrogen generation from the hydrolysis of Mg powder ball-milled with AlCl3. Energy. 2013 May;53:147–52. https://doi.org/10.1016/j.energy.2013.01.073

[30] Wang S, Sun L-X, Xu F, Jiao C-L, Zhang J, Zhou H-Y, et al. Hydrolysis reaction of ball-milled Mg-metal chlorides composite for hydrogen generation for fuel cells. International Journal of Hydrogen Energy. 2012 Apr;37(8):6771–5. https://doi.org/10.1016/j.ijhydene.2012.01.099

[31] Tegel M, Schöne S, Kieback B, Röntzsch L. An efficient hydrolysis of MgH2-based materials. International Journal of Hydrogen Energy. 2017 Jan;42(4):2167–76. https://doi.org/10.1016%2Fj.ijhydene.2016.09.084

[32] Tessier J-P, Palau P, Huot J, Schulz R, Guay D. Hydrogen production and crystal structure of ball-milled MgH2–Ca and MgH2–CaH2 mixtures. Journal of Alloys and Compounds. 2004 Aug;376(1–2):180–5. https://doi.org/10.1016/j.jallcom.2003.12.013

[33] Huot J, Liang G, Schulz R. Magnesium-based nanocomposites chemical hydrides. Journal of Alloys and Compounds. 2003 Apr;353(1–2):L12–5. https://doi.org/10.1016%2FS0925-8388(02)01306-3

[34] Tayeh T, Awad AS, Nakhl M, Zakhour M, Silvain J-F, Bobet J-L. Production of hydrogen from magnesium hydrides hydrolysis. International Journal of Hydrogen Energy. 2014 Feb;39(7):3109–17. https://doi.org/10.1016/j.ijhydene.2013.12.082

[35] Sun Q, Zou M, Guo X, Yang R, Huang H, Huang P, et al. A study of hydrogen generation by reaction of an activated Mg–CoCl2 (magnesium–cobalt chloride) composite with pure water for portable applications. Energy. 2015 Jan 1;79:310–4. https://doi.org/10.1016/j.energy.2014.11.016

[36] Liu P, Wu H, Wu C, Chen Y, Xu Y, Wang X, et al. Microstructure characteristics and hydrolysis mechanism of Mg–Ca alloy hydrides for hydrogen generation. International Journal of Hydrogen Energy. 2015 Mar;40(10):3806–12. https://doi.org/10.1016/j.ijhydene.2015.01.105

[37] Suryanarayana C. Mechanical alloying and milling. Progress in Materials Science. 2001 Jan 1;46(1):1–184. https://doi.org/10.1016%2FS0079-6425(99)00010-9

[38] TOPAS V4: General Profile and Structure Analysis Software for Powder Diffraction Data, User's Manual, Bruker AXS, Karlsruhe, 2008.

[39] Gennari FC, Castro FJ, Urretavizcaya G. Hydrogen desorption behavior from magnesium hydrides synthesized by reactive mechanical alloying. J Alloys Compd 2001;321:46-53. https://doi.org/10.1016/S0925-8388(00)01460-2.

[40] Li W, Li C, Zhou C, Ma H, Chen J. Metallic Magnesium Nano/Mesoscale Structures: Their Shape-Controlled Preparation and Mg/Air Battery Applications. Angew Chem Int Ed. 2006 Sep 11;45(36):6009–12. https://doi.org/10.1002/anie.200600099

[41] Höche D, Blawert C, Lamaka SV, Scharnagl N, Mendis C, Zheludkevich ML. The effect of iron re-deposition on the corrosion of impurity-containing magnesium. Phys Chem Chem Phys. 2016;18(2):1279–91. https://doi.org/10.1039/C5CP05577F

[42] Wei J, Zhou M, Long A, Xue Y, Liao H, Wei C, et al. Heterostructured Electrocatalysts for Hydrogen Evolution Reaction Under Alkaline Conditions. Nano-Micro Lett. 2018 Oct;10(4):75. https://doi.org/10.1007/s40820-018-0229-x